IV. Electrical Heating

Electrical preheating was previously employed during the DUSDP at TFF to warm clay layers. Then, two separate steam injection and vacuum extraction phases removed gasoline from the soil and ground water. In the application to this ARV phase, electrical heating was designed to target a particular region, a "cold spot," below the water table, which did not heat up sufficiently in the initial phases of electrical heating and steam injection. This cold spot, consisting of low-permeability soils below the water table, is near heating wells HW104 and HW103 as shown in Figure 18. The cold spot was identified during the drill-back characterizations carried out by the DUSDP in September 1993 (Newmark *et al.*, 1994).

Five different types of wells are shown in Figure 18. The GIW wells combine steam injectors with electrodes for soil heating and surround the bulk of the spill. The HW wells are for electrical heating only and have separate electrodes in the upper and lower clay units. The TEP wells are thermocouple monitoring wells. The GEW and GSW wells are extraction wells, which are located near the center of the pattern. Finally, the most recently drilled wells, HW-102, 103, 104, and 105, are DUSDP post-steam injection characterization wells that were completed as electrical heating wells for use in the ARV phase. The newer wells differ from earlier electrical heating wells in that the electrodes are longer (18 m instead of 3.05 m) and larger in diameter (11.4 cm instead of 6.3 cm) than the original HW or GIW electrodes. Details of the well designs and completions can be found in Newmark *et al.* (1994).

The new wells were placed to better target the cold spot, and the expected primary current paths and phasing are shown in Figure 19. Note that wells GIW-813, 818, and 819 were not used. Their electrodes were badly damaged during the electrical preheat phase of DUSDP.

Pre-DUSDP electrical soil heating started on November 30, 1993, and ended on December 13, 1993. Operations were conducted 24 h a day during the weekends of December 4 and 11 and only during the night on weekdays. The desired baseline configuration, shown in Figure 19 and consisting of 12 electrodes, was realized for only a fraction of the total running time. Values of interwell electrical resistance turned out to be too low for us to run the baseline configuration for voltages in excess of 208 volts AC (VAC). At voltages above this, we would exceed the 600-A current limit to the electrodes, which would trip the circuit breakers. When the new wells were installed, we did not upgrade the breakers or wiring to the electrodes and were thus limited to 600 A per electrode.

The operational strategy employed for the ARV phase of electrical heating was based on knowledge gained from the electrical heating phase of DUSDP. That is, the region around an electrode will dry out as it warms up and the warming vaporizes water. When this happens, the interwell resistances will increase and seek to limit the current. Thus, we proceeded by using some subset of the baseline configuration until resistances increased (and currents dropped). We then added an additional well and heated it until currents dropped sufficiently to add yet another well. This process was repeated until we could proceed no further because of excess current levels. Using this strategy, we were able to use all 12 electrodes at 208 VAC and 11 out of 12 electrodes at 350 VAC. We were not able to operate with the voltage above 350 VAC.

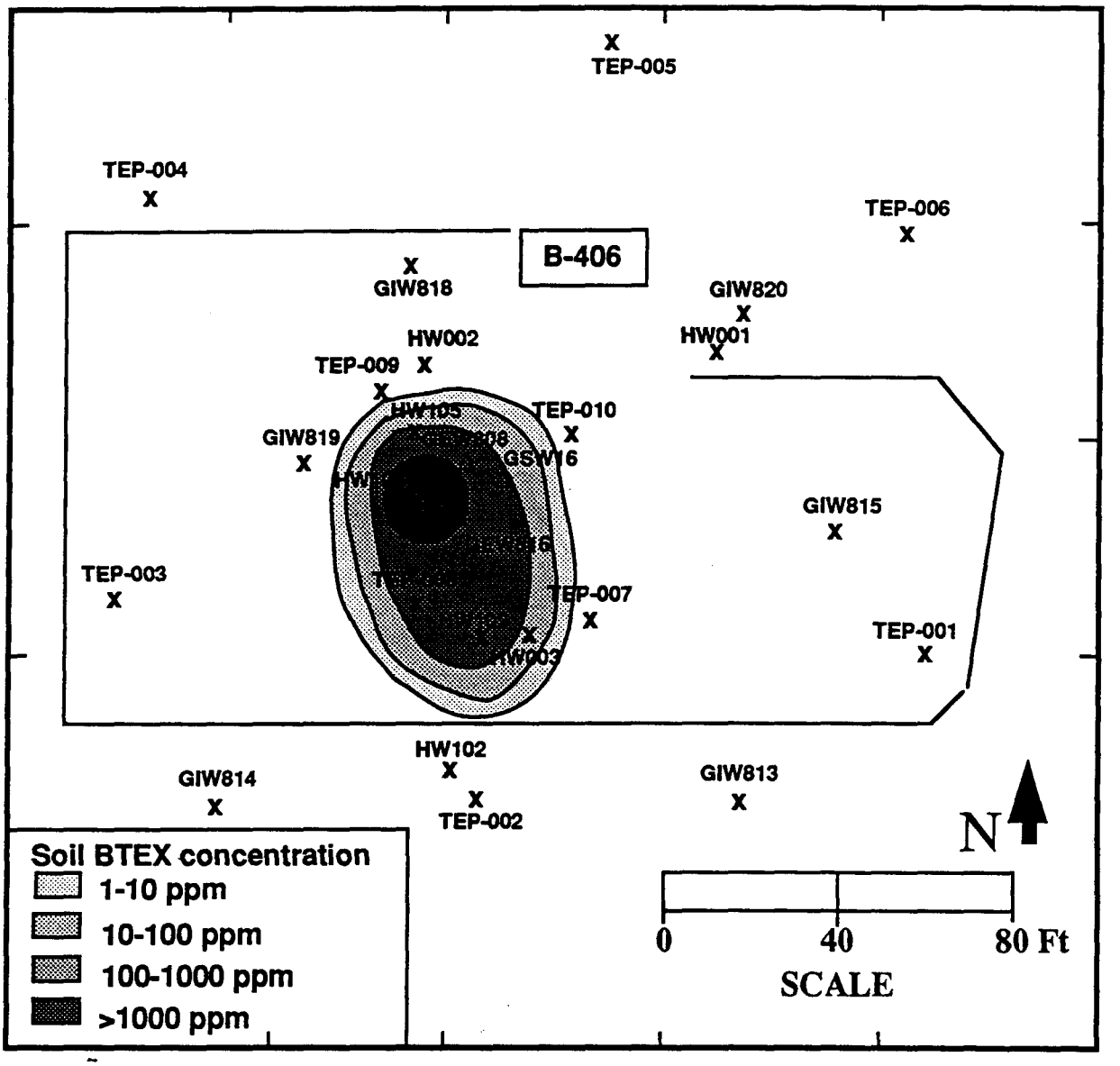

Figure 18. Plan view of the TFF site showing locations of wells of interest for the electrical heating activities. The "cold spot" in the clay aquitard is identified by the area with the highest remaining contamination levels after the DUSDP (figure made using data from Newmark *et al.*, 1994).

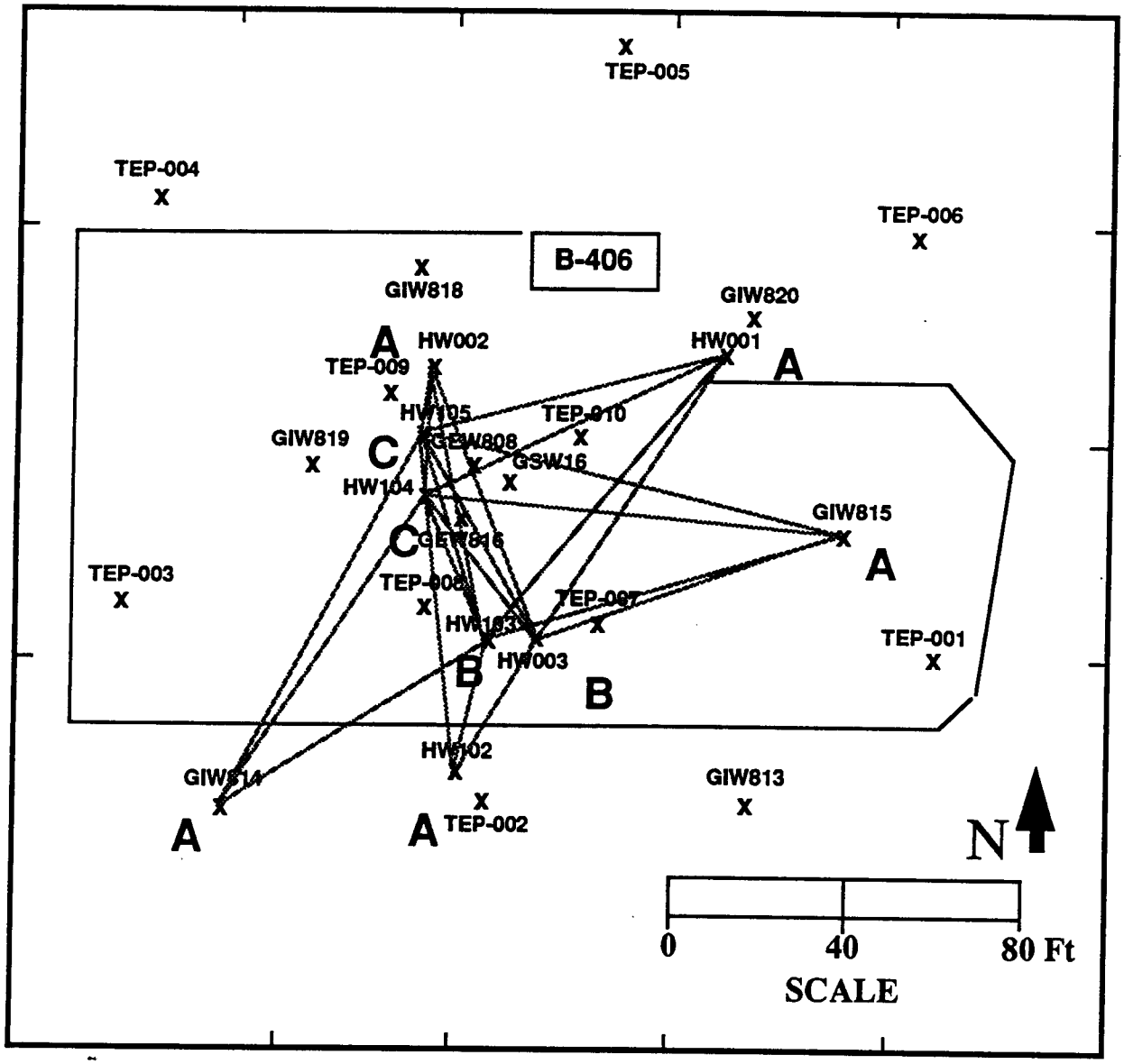

Figure 19. Same plan view as Figure 18, with the inclusion of path lines showing electrical paths available between different heating wells used in the electrical heating operations.

During the course of the heating, about 44,300 kW-h of energy were delivered through the electrodes. In the most productive well, HW-103, 9,145 kW-h of energy were deposited, and in the least productive, HW-002 (upper zone), 716 kW-h were deposited. Total power dissipation reached a maximum of 450 kW with an average value of 221 kW.

Temperatures were logged with the automated data acquisition system (Appendix 3 and Newmark *et al.*, 1994). The results are presented in the plots of Figures 20 to 24 for TEP wells 2, 7, 8, 9, and 10. Each of these TEP wells has four fixed thermocouples, TCs 1 to 4, located at depths of 130 ft, 110 ft, 95 ft, and 80 ft, respectively.

Let us now examine the thermocouple data for evidence of warming. Note that thermocouple 1 at the 130-ft depth is below the water table and significantly cooler than the other thermocouples for all of the TEP wells. For the most part, thermocouples 2, 3, and 4 are in the 80° to 90°C range, even many months after steaming.

First, consider TEP 2, which is shown in Figure 20. Thermocouple 1 appears to show the effect of ground water pumping very clearly. During pumping, as cool water is drawn in from the surrounding areas, the temperature decreases (see also Section I above and Fig. 9). When pumping stops, the temperature increases, probably due to conductions from warm soil nearby. Thermocouple 2 is always cooling, though the rate of cooling slows during heating. Thermocouples 3 and 4 clearly show an increase in temperature of around 4°C due to electrical heating. TEP 2 is only about 3 m away from HW-102.

The temperature plots for TEP 7 are shown in Figure 21. Thermocouple 1 appears to respond to ground water pumping, though not as strongly as TEP 2. Thermocouples 2, 3, and 4 appear to be unaffected by electrical heating or ground water pumping. The heating well nearest to TEP 7 is HW-003, which is about 5.2 m away.

Figure 22 shows the temperature plots for TEP8. As before, thermocouple 1 responds to ground water pumping. Thermocouple 2 shows a temperature increase of about 3°C due to electrical heating. Thermocouples 3 and 4 show a strange temperature increase, which appears to occur just when electrical heating is stopped The origin of this increase is not understood. The heating well nearest to TEP 8 is HW-103 at a distance of about 3.5 m.

Temperature plots for TEP 9 (Fig. 23) are similar to those for TEP7 and TEP8. Thermocouple 1 responds to ground water pumping. Thermocouple 2 cools slowly when electrical heating is off and warms slowly when the heating is on. Thermocouples 3 and 4 cool slowly whether heating is on or off. TEP 9 is about 3.35 m away from HW-105 and 3.66 m away from HW-002.

In Figure 24, we see that thermocouple 1 in TEP 10 responds to pumping in a way generally opposite to the other TEP wells. Its temperature increases during pumping and decreases without pumping. Thermocouples 2, 3, and 4 vary only a little, though thermocouple 2 appears to cool slowly after heating is turned off while thermocouples 3 and 4 appear to warm slowly.

A rough estimate of the expected heating effect can be made by assuming that the soil at the TFF site is "average." The volumetric heat capacity for average soil (Carslaw and Jaeger, 1959) is 0.56 kW-h/m^3-°C. Given the energy input of 44,300 kW-h, the heating effect can be expressed

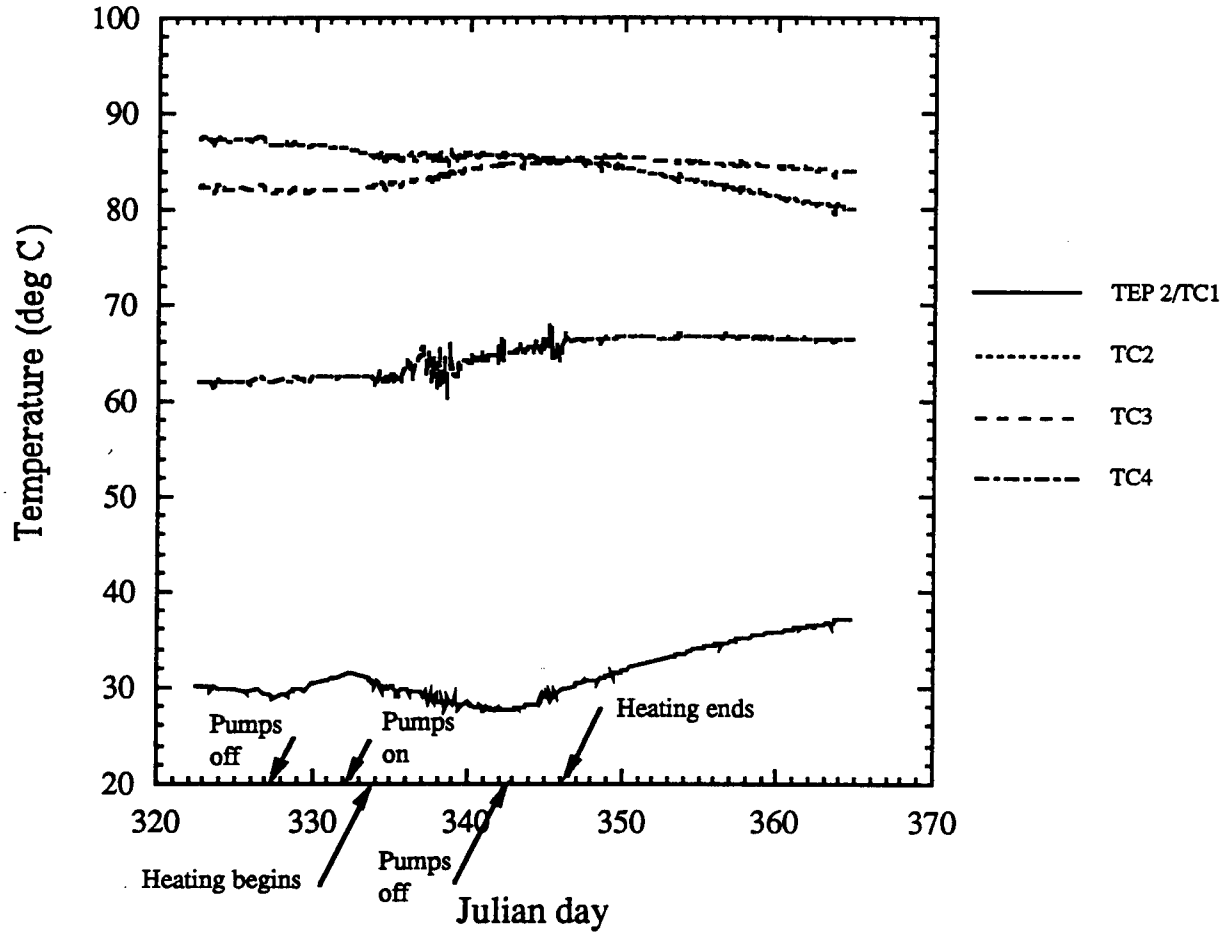

Figure 20. Temperatures at well TEP2 before, during, and after the electrical heating phase of ARV. Arrows show when ground water pumping started and stopped and when electrical heating started and stopped.

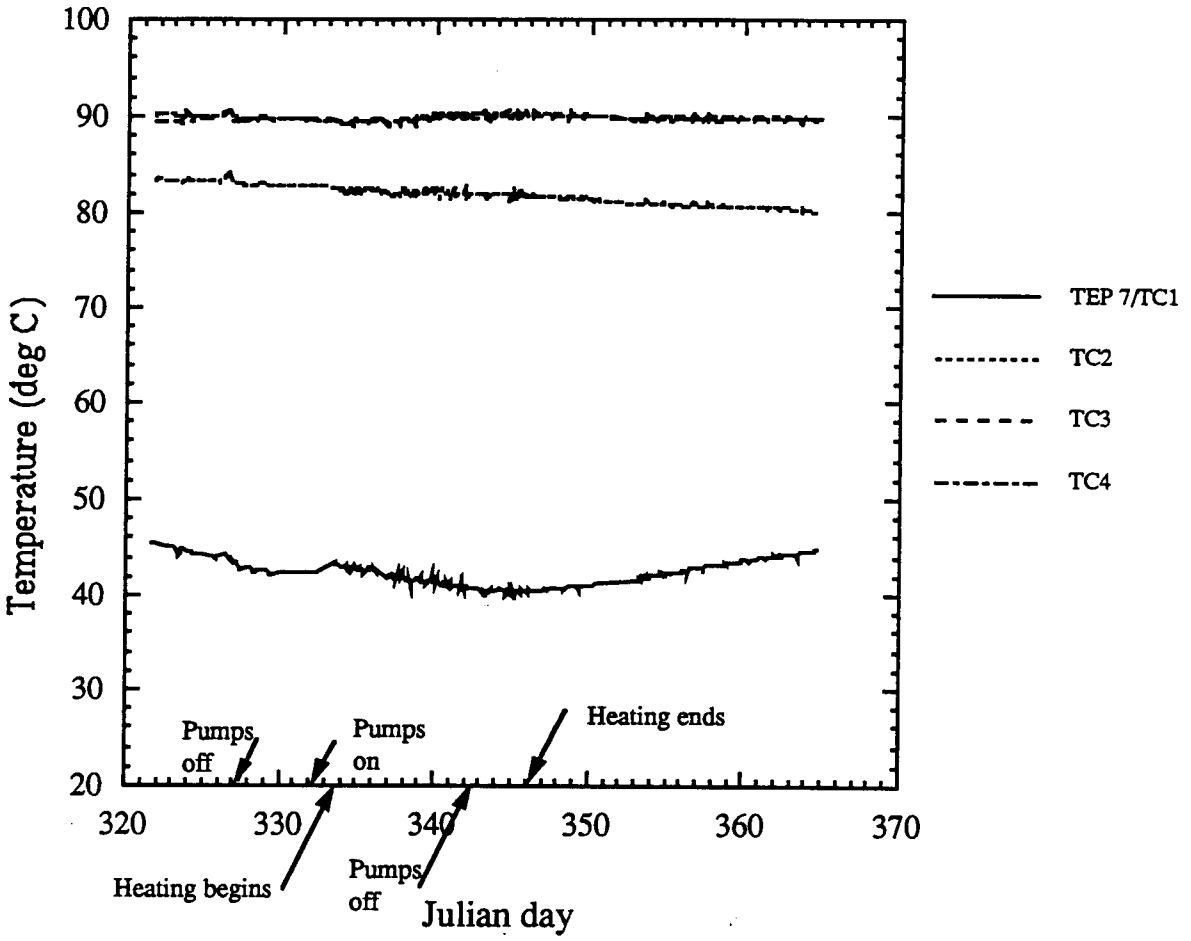

Figure 21. Temperatures at well TEP7 before, during, and after the electrical heating phase of ARV. Arrows show when ground water pumping started and stopped and when electrical heating started and stopped.

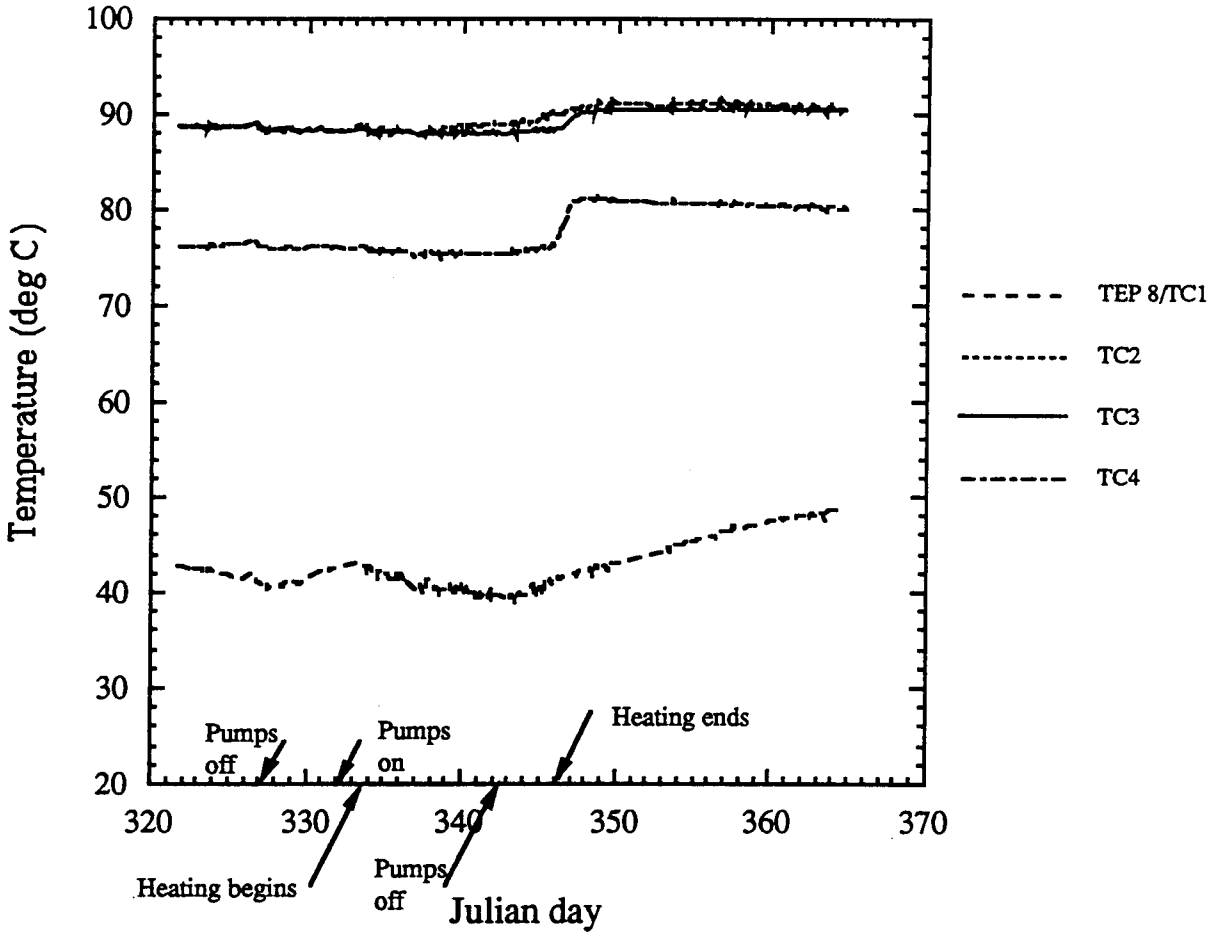

Figure 22. Temperatures at well TEP8 before, during, and after the electrical heating phase of ARV. Arrows show when ground water pumping started and stopped and when electrical heating started and stopped.

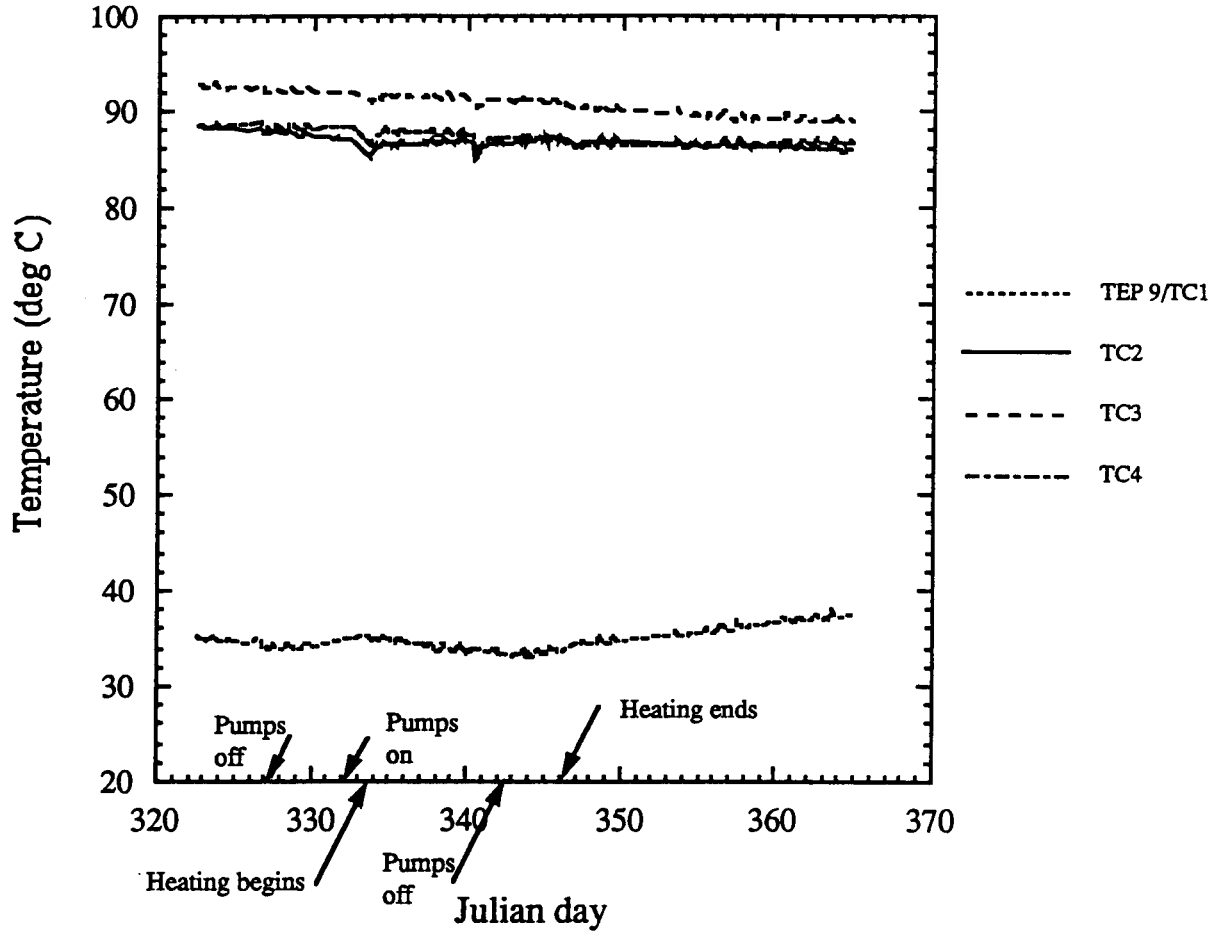

Figure 23. Temperatures at well TEP9 before, during, and after the electrical heating phase of ARV. Arrows show when ground water pumping started and stopped and when electrical heating started and stopped.

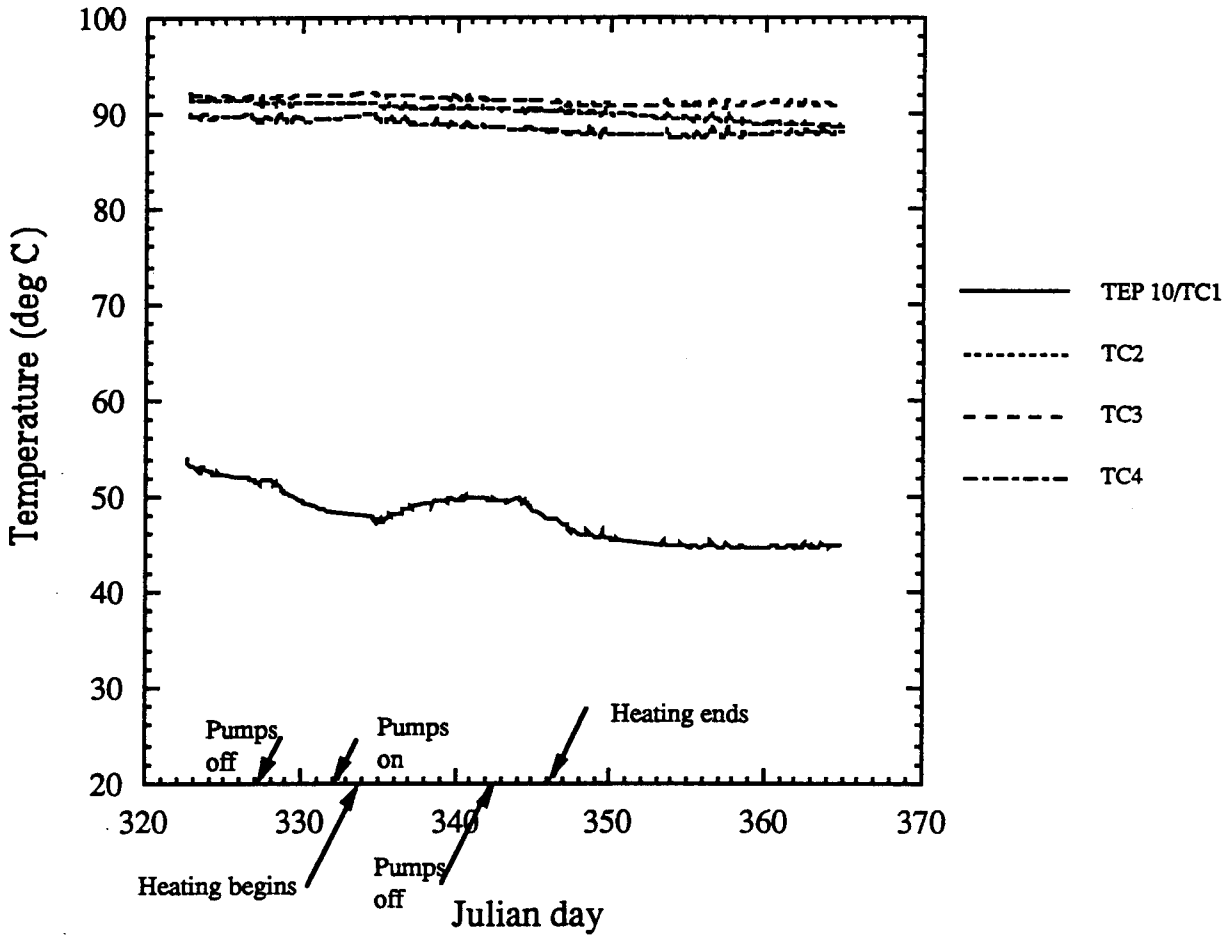

Figure 24. Temperatures at well TEP10 before, during, and after the electrical heating phase of ARV. Arrows show when ground water pumping started and stopped and when electrical heating started and stopped.

by a volume-temperature product of 79,100 m^3-°C. If the volume heated is taken to be 18 m (60 ft) in height (the electrode length) and bounded by TEP wells 2, 7, 8, 9, and 10, then the volume is 4,706 m^3 and the expected temperature rise is about 79,100/4,706°C, or 16.8°C. From the temperature plots, temperature increases attributable to heating are obviously a few degrees at most. Where then did all of the energy go?

An examination of the data for condensate produced during electrical heating provides a plausible explanation. The data are presented in Figure 25 and show high condensate collection rates when heating is on, and low collection rates when off. When these data are compared with the energy input versus time of Figure 26, a pulse of condensate seems to be produced each time the heating comes on.

The total condensate collected during electrical heating was 33,085 gals. Of this, about 2,700 gal is what would normally be collected without electrical heating (background). Thus, about 30,385 gal of condensate may be attributed to electrical heating. The energy required to vaporize this amount of water is about 80,000 kW-h. This figure is nearly twice that for the input electrical energy and needs more explanation, but the main point is: most of the input energy probably went to vaporize water and not to heat soil.

There is a plausible mechanism for this large vapor production. Consider the situation depicted in Figure 27. Here, two long electrodes (18 m), like the ones used in HW-102, 103, 104, and 105, are placed in a layered soil as shown. This represents the kind of situation at the LLNL gasoline spill. When a voltage is applied between the electrodes (in the model), current flows and the region around the electrodes begins to warm. Steam is produced at the electrodes and moves readily into the upper steam zone (USZ). This has the effect of greatly increasing the electrical conductivity of the USZ relative to the confining clay layer (CON) beneath. As a result, current flows preferentially into the USZ, which heats rapidly to temperatures of 100°C while the clay has warmed only about 5°C.

The above ideas were incorporated into a simulation using the NUFT computer code. The results of this modeling, though preliminary, indicate that it is not good practice to have long electrodes that extend into permeable zones if the object is to heat the clay zones. Details of the modeling work are presented in Appendix 5.

The electrical heating phase of ARV did not produce the desired heating. There were several contributing factors. The first, and perhaps the most important, was that the new electrodes in wells HW-102, 103, 104, and 105 were too long and not properly placed to target the desired clay zone. Because the electrodes extended into the upper and lower steam zones, large quantities of steam formed at the electrodes, and most of the input energy went into making steam. Additionally, when the steam moved into the steam zones, it made them highly conductive and diverted current from the clay zones to the steam zones. The overall result was that the target clay zones heated very slowly, if at all.

Another factor contributing to the poor heating rates was the mismatch between system impedance and the wiring and breakers to the new heating wells, HW-102, 103, 104, and 105. The wiring and safety circuit breakers were limited to 600 A. The electrodes in these wells were capable of much higher currents, had we been able to use the available secondary voltages of 480 and 600 VAC.

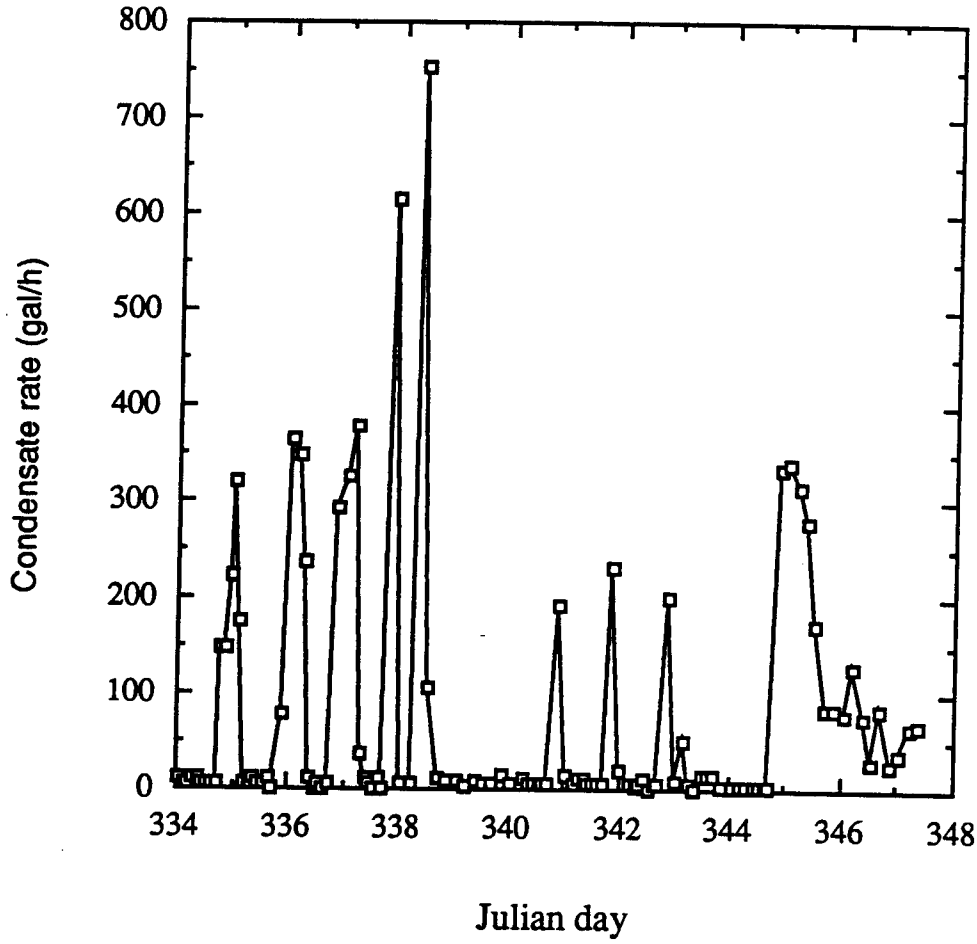

Figure 25. Plot of the rate of condensate recovery in the extracted vapor, in gal/h, as a function of time (Julian day) during the electrical heating phase of ARV. Most of the recovery appears as spikes that occur during overnight or week-end electrical heating activities.

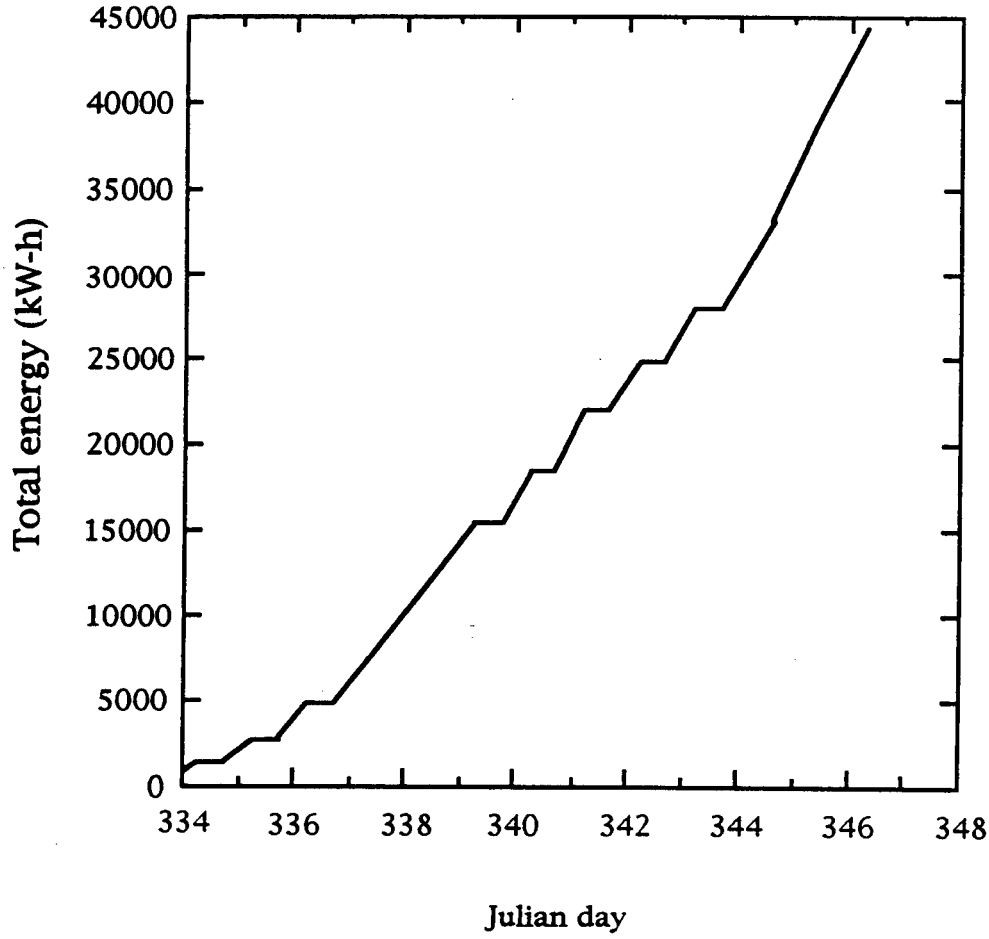

Figure 26. Cumulative energy deposition into electrodes, in kW-h during the electrical heating part of ARV. Compare with Figure 25, and note that most of the increases in energy (i.e., electrical energy was being applied) correlate with peaks in condensate recovery.

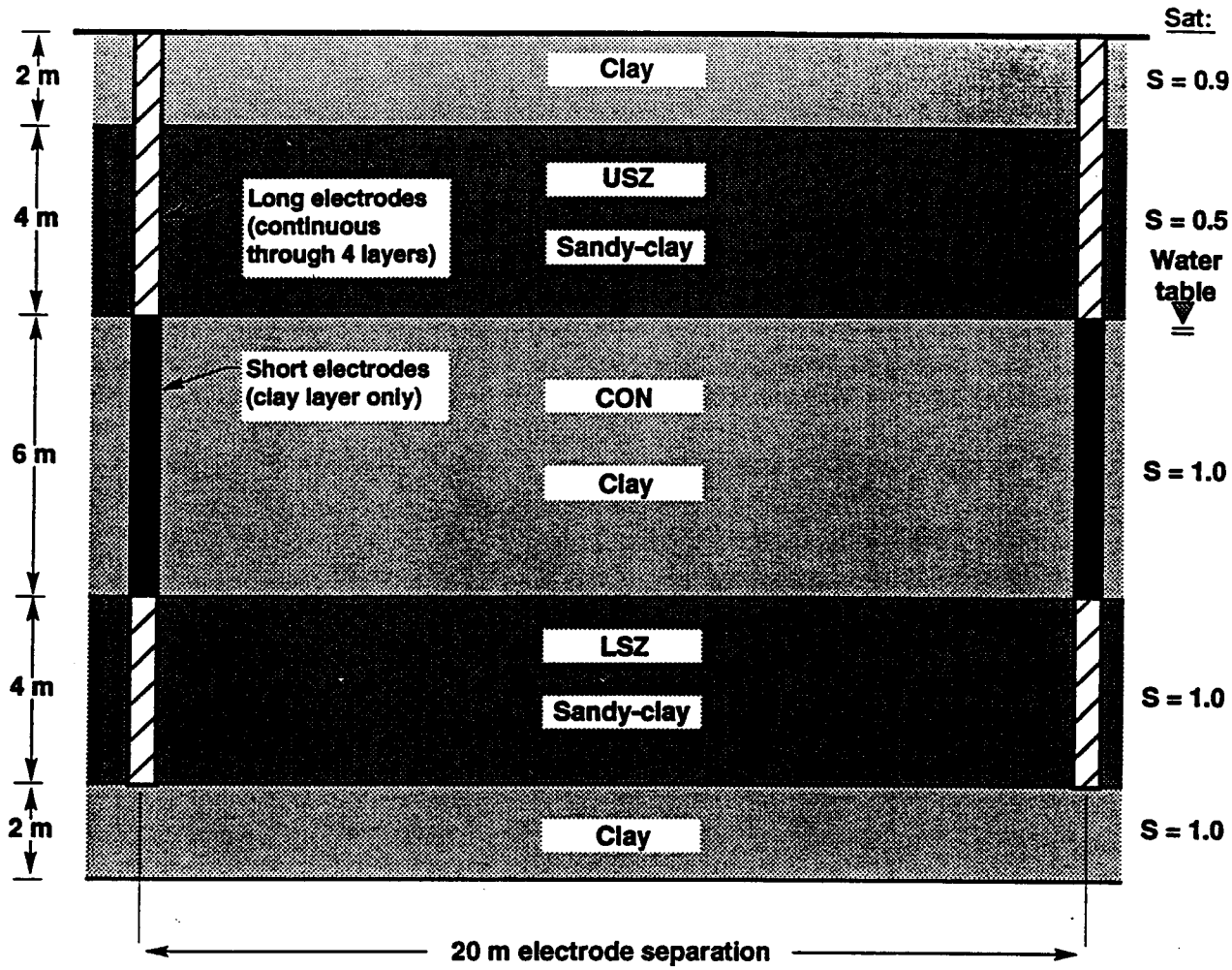

Figure 27. Simplified diagram of subsurface geology of heater wells at the TFF site which shows the size of the installed heater electrodes and their as-installed relation to the formation. The short electrodes (solid black) were installed and used during the DUSDP and the ARV phases of activities. The long electrodes (diagonal strips) were installed after the DUSDP in drill-back characterization wells and used exclusively during the ARV phase.

ERT images were also run before and after the electrical heating. Figure 28 shows difference images between data taken on October 27 to 29 and December 13. Note that continuous pumping (with the exception of the Thanksgiving hiatus and the last 4 days) of ground water was carried out during this time and accounts for the largest effect seen on the ERT images. The TEP2-TEP8 and TEP2-TEP7 cross sections show a large area of higher resistivity correlated with zones of high permeability. This is undoubtedly caused by the influx of cold water during pumping (see also Fig. 9). Cooler temperatures will cause resistivity to increase. Other influences, such as the vertical column of increased resistivity seen in TEP2-TEP8 and TEP9-TEP7, may be related to drying of the formation near the electrodes during electrical heating. There is no evidence in the images that specific clay layers have been significantly heated.

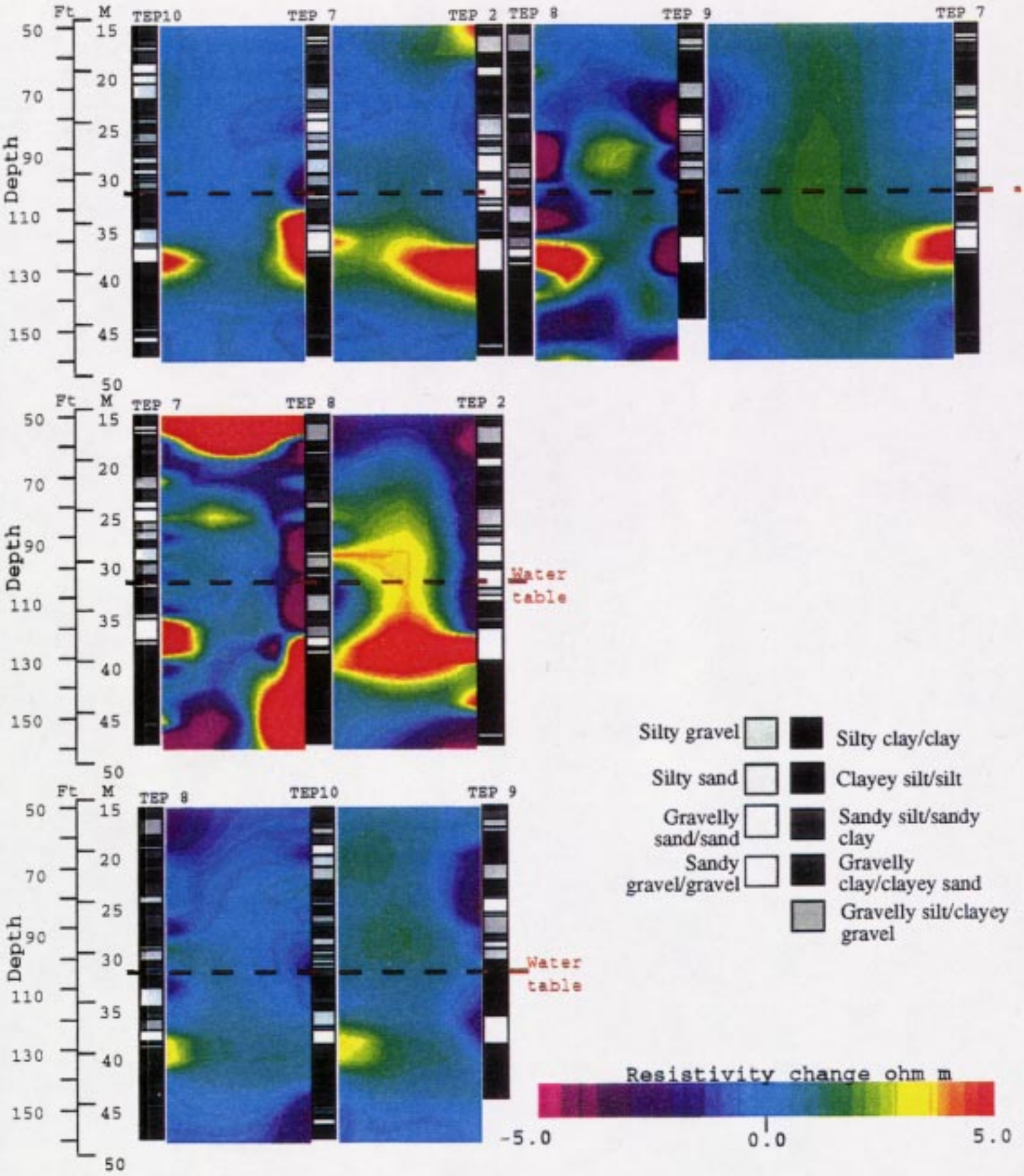

Figure 28. Electrical resistance tomography (ERT) images made at the end of electrical heating.